**ORIGINAL ARTICLE**

# Study on the distribution characteristics of stress deviator in the surrounding rock when mining closely spaced coal seams

Renliang Shan[1] · Zhaolong Li[1] · Chunhe Wang[1,2] · Yonghui Wei[1] · Xiao Tong[1] · Shuai Liu[1] · Zhonghao Shan[1]

## Abstract

In mining closely spaced coal seams, the roadway arrangement for gas drainage in lower coal seams is always a concern. This paper uses mechanical model calculations and numerical simulation postprocessing methods to study the stress deviator distribution characteristics of the surrounding rock in the gob under various conditions. By calculating the distribution of the stress deviator, a reasonable location for the gas drainage roadway in engineering construction is determined, and the rationality of the roadway location selection is verified by the changes in the stress deviator in the surrounding rock during the mining of the lower coal seam. The research includes the following main results. (1) The theoretical formulas for vertical, horizontal, shear and stress deviator under a single gob of an inclined coal seam are derived through the semi-infinite body solution, and the stress deviator distributions in the roof and floor of the coal seam below the gob are calculated. The main factors affecting the distribution of stress deviator are determined by the following parameters: coal seam depth $H$, horizontal lateral pressure coefficient $\lambda$ and coal seam inclination $\theta$. (2) Through FLAC3D model calculation and postprocessing, the stress deviator distributions under different conditions are obtained, and the influences of various factors on the stress deviator distribution below a gob are analyzed. (3) Using the calculated theoretical results for the stress deviator and the distribution of the stress deviator obtained by the numerical method, the position of the gas drainage roadway during the mining of the upper coal seam is preliminarily selected; using numerical simulation of mining the lower coal seam, the stress deviator distributions in the surrounding rock during the mining of the lower coal are obtained, thus verifying the scientific basis and rationality of the gas drainage roadway layout.

**Keywords** Closely spaced coal seams · Geological factor · Stress deviator · Roadway layout · Gas drainage

## Introduction

Closely spaced coal seams (Yang et al. 2019; Cheng et al. 2020) are coal seams that interact with each other during mining process due to the short distance between the seams. China is rich in coal resources, and the reserves of close coal seams (Ma et al. 2015) account for a large proportion of coal seams. Unlike single coal seam mining, the mining of closely spaced coal seams is a complicated space problem involving the stability of the lower coal seam mining

roadway. This is mainly because, on the one hand, the caved gangue and residual coal pillars after the upper coal seam is mined cause uneven stress in the floor, and the stress concentration near the edge of a coal pillar is obvious. On the other hand, the rock surrounding the lower coal seam is affected by upper mining, which causes different degrees of damage and destruction, thereby resulting in the plastic failure of the surrounding rock, the development of cracks, and poor integrity. In response to this problem, many scholars around the world have conducted research by means of theoretical derivations (Das et al. 2019), numerical simulations (Toraño et al. 2002; Shang et al. 2019; Shabanimashcool and Li 2012) and field measurements.

The main factors affecting the stability of the roadway include the stress state in the surrounding rock, the strength of the surrounding rock and the support form of the roadway. To explore the stress state and strength of the surrounding rock during the mining of closely spaced coal seams, Zhang

✉ Zhaolong Li
cumtblzl@163.com

1　School of Mechanics and Civil Engineering, China University of Mining and Technology (Beijing), Beijing 100083, China

2　China Construction Communications Engineering Group Corporation Limited, Beijing 100161, China

et al. (2014) used a mechanical model established by the infinitesimal strain method to study the reasons for the failure and instability of the surrounding rock. Suchowerska et al. (2013, 2014) calculated the vertical and horizontal stresses in the floor during longwall mining. Zhang et al. (2018) studied the depth of damage to the surrounding rock caused by coal mining. Bai et al. (2014) conducted numerical simulation analysis and investigations and observed fragmentation of the rock surrounding the roadway under the influence of mining. Tan et al. (2010) divided the floor damage caused by coal seam mining into four failure zones. Liu et al. (2016) used numerical simulation to study the stress state in the rock surrounding the coal seam before and after mining and proposed that the roadway of the lower coal seam should avoid the area of stress concentration during close coal seam mining. Yan et al. (2015) determined the reasonable location of the roadway in the lower coal seam through stress calculations and numerical calculations. In addition, Xu et al. (2019), Jiang et al. (2015) and other scholars (Wang et al. 2017, 2016) improved the stability of the rock surrounding the roadway by optimizing the roadway support method.

Research and analysis of the stress distribution in the rock surrounding the lower coal seam show that avoiding arranging roadways in high stress concentration areas is the key to ensuring the stability of the lower coal roadways in mining close coal seams (Li et al. 2016). However, most of the existing research results take vertical stress as the main research object and ignore factors, such as horizontal stress, shear stress and strain energy density in the surrounding rock. In elastic–plastic mechanics, the rock mass stress tensor is divided into the spherical stress tensor and the stress deviator tensor (Tian et al. 2020). The second invariant $J_2$ of stress deviator (Li et al. 2020; Kroon and Faleskog 2013), can represent the distortion energy density of the rock mass and reflect the stability of the rock mass. Therefore, this paper uses the second invariant $J_2$ of the stress deviator to characterize the stress deviator and studies the distribution characteristics of the stress deviator in the surrounding rock under the influence of various factors; this approach has significance for the mining of close coal seams under different geological conditions.
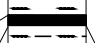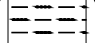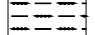
## Project summary

The Malan Mine is located in the central part of Shanxi Province, China, and is a high-gas mine. The 10606 longwall panel mined has a thickness of 2.1 m and a burial depth of approximately 400 m, and belongs to the #02 coal seam. The immediate roof and immediate floor are mudstone and sandstone, respectively, and the coal seam has inclination angles of 1–9°. The #2 coal seam is located 7 m below the #02 coal seam and has a thickness of 2.2 m. The immediate roof and immediate floor are silty mudstone and siltstone, respectively. The lithologies of the roof and floor are shown in Fig. 1.

The 10606 longwall panel is located in the #02 coal seam, and mining will be completed. The excavation of a gas drainage roadway (Aguado and Nicieza 2007; Cao et al. 2001) in the #2 coal seam below 10606 is planned; the gas in the 10606 gob, 10608 longwall panel and #2 coal seam will be extracted, and the roadway will be used for later mining of the #2 coal seam to achieve "one roadway with multiple uses". The coal field is a high-gas coal field, and excavations of many gas drainage roadways under many panels of the #02 coal seam are planned. This paper takes the 10606 panel and 10608 gas drainage roadway as an example, and the study of stress deviator is expected to provide a theoretical basis for laying out gas drainage roadways in this mining area.

**Fig. 1** Columnar section of the rock strata

| Thickness/m | Lithology | Strata | Rock features |
|---|---|---|---|
| 6.05 | | Silty mudstone | Dark gray, thickly layered |
| 2.14 | | #02 Coal | Black, lumpy, poor lithology |
| 4.97 | | Sandstone | Off-white medium-fine sandstone, mainly quartz and feldspar |
| 0.45 | | #1 Coal | Black, containing sandy mudstone |
| 1.49 | | Silty mudstone | Dark gray, containing pyrite film |
| 2.20 | | #2 Coal | Black, semibright coal, blocky |
| 1.89 | | Siltstone | Gray, containing fossilized plant roots |
| 0.49 | | #3 Coal | Black, semibright coal, blocky |
| 5.00 | | Silty mudstone | Dark gray |

The layout of the 10606 and 10608 longwall panels is shown in Fig. 2. Figure 2a shows the layout of the panels in the horizontal plane and some geological structures (such as faults and collapsed columns). Figure 2b shows the relationship of the panels in the vertical plane. Due to the long service life of the roadway and the tasks of both gas drainage and later mining of the #2 coal seam, when selecting the location of the roadway, not only the stress environment of the rock mass but also the reasonable planning of the entire mining district must be considered.
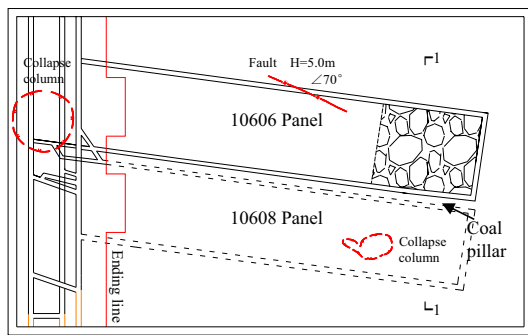


**(a)** Layout of longwall panel
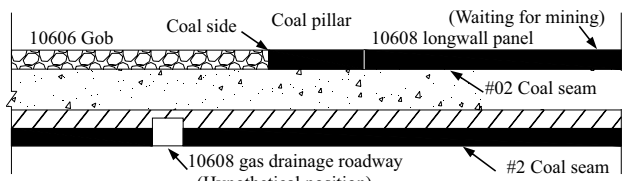


**(b)** Section at 1-1

**Fig. 2** Arrangement of the longwall panel

# Theoretical calculation of stress deviator

According to mine pressure theory, after a coal seam is mined to form a gob, the overburden in the gob is damaged and collapses. A large-scale vertical stress relief zone appears under the gob, and a vertical stress concentration area is formed near the edge of the coal pillar. As the distance between the rock mass and the gob increases, the vertical stress gradually returns to the original rock stress. Due to the redistribution of stress after the coal seam is excavated, the second invariant $J_2$ of the stress deviator in the floor changes significantly. In this section, the second invariant $J_2$ formula of the stress deviator below the inclined gob is obtained using the semi-infinite elastic body solution, and the main factors affecting the stress deviator are analyzed.

## Theoretical calculation of the floor stress below the inclined gob

Many scholars (Sun et al. 2019; Zhu et al. 2017a, b) around the world have performed much research on calculating floor stress during the mining of close coal seams. Considering a variety of conditions, this section theoretically derives the floor stress after the inclined coal seam is mined.

According to the distribution of the lateral abutment pressure (Brady and Brown 1993) on the longwall working face, the lateral abutment pressure acting on the surrounding rock can be approximated as a triangular distribution. The surrounding rock mass in the gob is regarded as a semi-infinite ideal elastic body (Suchowerska et al. 2013; Zhang et al. 2018), and the abutment pressure increment caused by mining is simplified to obtain the mechanical model of the lateral abutment pressure increase of the gob, as shown in Fig. 3a.

As shown in Fig. 3, a simplified mechanical calculation model (Fig. 3b) is constructed with the direction parallel to the floor as the x-axis and the direction perpendicular
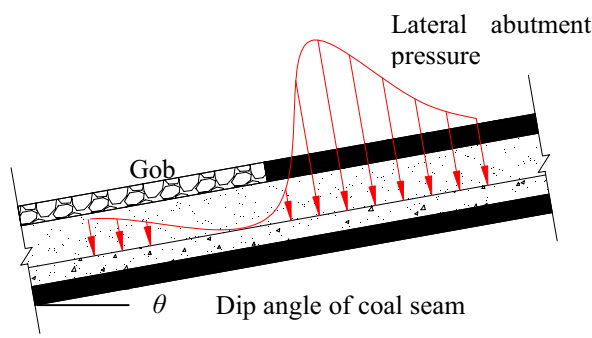


**(a)** Lateral abutment pressure distribution
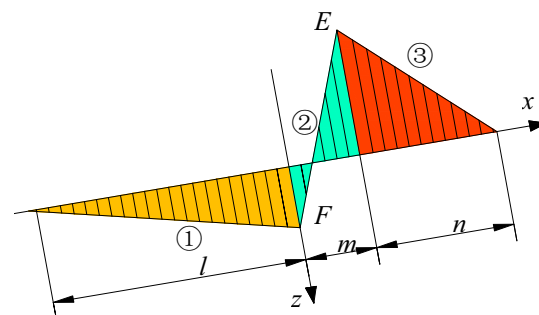


**(b)** Simplified mechanical calculation model

**Fig. 3** Model for calculating the floor stress increment

to the floor as the $z$-axis; the inclination angle of the coal seam is $\theta$ (suitable for coal seams with small dip angles). To facilitate the integration operation, the distribution range of the stress increment is divided into three regions. Area ①, whose length is denoted by $l$, is the region affected by the additional stress under the gob; area ②, whose length is denoted by $m$, is the area between the coal side and the peak lateral abutment pressure; and area ③, whose length is denoted by $n$, is the range from the peak lateral

abutment pressure to the original rock stress zone. $E$ represents the maximum additional stress under the coal pillar $((K-1)\cdot\gamma H\cdot(\cos\theta + \lambda\sin\theta))$, and $F$ represents the maximum additional stress under the gob $(-\gamma H\cdot(\cos\theta + \lambda\sin\theta))$.

The additional stresses ①, ② and ③ in the floor are integrated, and the additional vertical, horizontal and shear stresses in the rock surrounding the floor in the three regions are superimposed on the original rock stress field to obtain the stress formula for any point $Q(x, z)$ below the floor:

$$\sigma_z = \gamma H(\cos\theta + \lambda\sin\theta) \cdot \left\{ \begin{array}{l} \left(\dfrac{x+l}{\pi a}\right)\left[\begin{array}{l} \dfrac{xz}{x^2+z^2} - \dfrac{(x+l)z}{(x+l)^2+z^2} \\ + \arctan\dfrac{x}{z} - \arctan\dfrac{x+l}{z} \end{array}\right] + \\ \left(\dfrac{m-Kx}{\pi m}\right)\left[\begin{array}{l} \dfrac{(x-m)z}{(x-m)^2+z^2} - \dfrac{xz}{x^2+z^2} \\ + \arctan\dfrac{x-m}{z} - \arctan\dfrac{x}{z} \end{array}\right] + \\ \left[\begin{array}{l} \dfrac{(x-m-n)z}{(x-m-n)^2+z^2} - \dfrac{(x-m)z}{(x-m)^2+z^2} \\ + \arctan\dfrac{x-m-n}{z} - \arctan\dfrac{x-m}{z} \end{array}\right] \times \\ \left[(1-K)\dfrac{m+n-x}{\pi n}\right] + 1 \end{array} \right\} \tag{1}$$

$$\sigma_x = \gamma H(\cos\theta + \lambda\sin\theta) \cdot \left\{ \begin{array}{l} \left(\dfrac{x+l}{\pi l}\right)\left[\begin{array}{l} \dfrac{(x+l)z}{(x+l)^2+z^2} - \dfrac{xz}{x^2+z^2} \\ + \arctan\dfrac{x}{z} - \arctan\dfrac{x+l}{z} \end{array}\right] + \\ \left(\dfrac{m-Kx}{\pi m}\right)\left[\begin{array}{l} \dfrac{xz}{x^2+z^2} - \dfrac{(x-m)z}{(x-m)^2+z^2} \\ + \arctan\dfrac{x-m}{z} - \arctan\dfrac{x}{z} \end{array}\right] + \\ \left[\begin{array}{l} \dfrac{(x-m)z}{(x-m)^2+z^2} - \dfrac{(x-m-n)z}{(x-m-n)^2+z^2} \\ + \arctan\dfrac{x-m-n}{z} - \arctan\dfrac{x-m}{z} \end{array}\right] \times \\ \left[(1-K)\dfrac{m+n-x}{\pi n}\right] + \dfrac{\sin\theta + \lambda\cos\theta}{\cos\theta + \lambda\sin\theta} \end{array} \right\} \tag{2}$$

$$\tau_{xz} = \gamma H(\cos\theta + \lambda\sin\theta) \cdot \left\{ \begin{array}{l} \left(\dfrac{x+l}{\pi l}\right)\left[\dfrac{z^2}{(x+l)^2+z^2} - \dfrac{z^2}{x^2+z^2}\right] + \left(\dfrac{Kx-m}{\pi m}\right)\left[\dfrac{z^2}{(x-m)^2+z^2} - \dfrac{z^2}{x^2+z^2}\right] \\ + \left[(K-1)\dfrac{m+n-x}{\pi n}\right] \times \left[\dfrac{z^2}{(x-m-n)^2+z^2} - \dfrac{z^2}{(x-m)^2+z^2}\right] \end{array} \right\} \tag{3}$$
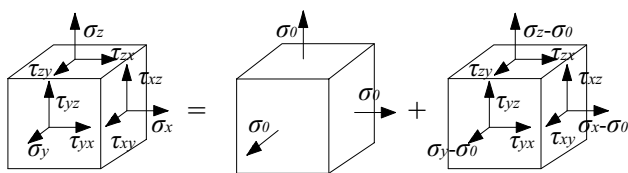
**Fig. 4** Stress decomposition of a rock mass unit

In the formula, $\gamma$ is the volume weight of the overburden, $H$ is the depth of the coal seam, $\lambda$ is the horizontal pressure coefficient, $K$ is the maximum stress concentration factor, and $\theta$ is the inclination angle of the coal seam.

## Theoretical calculation of the stress deviator below the gob

The stress tensor $\sigma_{ij}$ of the rock mass can be decomposed into two parts: the spherical stress tensor $\sigma_0 \delta_{ij}$ and the stress deviator $s_{ij}$. The spherical stress tensor represents the state of equal stress in all directions and generally causes only elastic deformation, while the stress deviator causes inelastic deformation of the rock mass, as shown in Fig. 4:

$$
\begin{cases}
\sigma_{ij} = \begin{bmatrix} \sigma_x & \tau_{xy} & \tau_{xz} \\ \tau_{yx} & \sigma_y & \tau_{yz} \tau_{yz} \\ \tau_{zx} & \tau_{zx} & \sigma_z \end{bmatrix} = \sigma_0 \delta_{ij} + s_{ij} \\
\sigma_0 = (\sigma_1 + \sigma_2 + \sigma_3)/3 \\
\delta_{ij}(i,j = x,y,z) = \begin{cases} 1 & (i = j) \\ 0 & (i \neq j) \end{cases}.
\end{cases}
\tag{4}
$$

In elastic–plastic mechanics, the second invariant $J_2$ of the stress deviator can effectively express the distortion energy density and the stability of the rock mass and material. When the deviation between the actual stress state and the average stress state is greater, the stress deviator is higher, and yield failure is more likely to occur. Therefore, the second invariant $J_2$ of the stress deviator is adopted in this paper

to represent the stress deviator in the rock surrounding the stope to provide a basis for selecting the location of the gas drainage roadway under the gob.

$$
J_2 = \frac{1}{6}\left[(\sigma_x - \sigma_y)^2 + (\sigma_y - \sigma_z)^2 + (\sigma_z - \sigma_x)^2\right] + (\tau_{xy}^2 + \tau_{yz}^2 + \tau_{zx}^2)
\tag{5}
$$

Simultaneous formulas (1), (2), (3), and (5) can be used to obtain the stress deviator in the rock surrounding the gob. The theoretical calculation results for the stress deviator in the roof and floor of the lower coal seam (the #2 coal seam) are shown in Fig. 15. The formulas illustrate that the significant change in the stress state of the surrounding rock caused by mining and other reasons is the fundamental cause of the change in the stress deviator. According to the theoretical formula, the main factors that affect the stress deviator in the surrounding rock include the coal seam depth $H$, horizontal pressure coefficient $\lambda$, and inclination angle $\theta$ of the coal seam.

## Stress deviator distribution characteristics

Based on the distribution of rock layers in the Malan Mine, FLAC3D software is used to establish a numerical model of the mining of closely spaced coal seams to study the distribution characteristics of the stress deviator in the rock surrounding the gob under different coal seam depths,
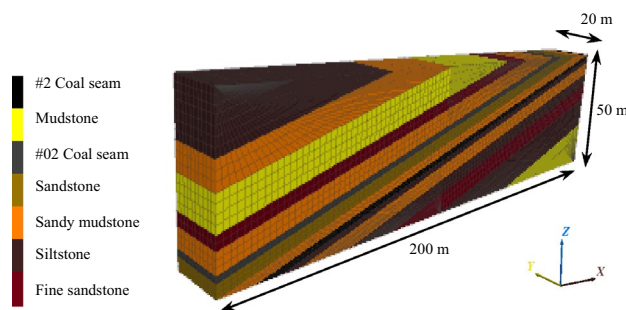


**Fig. 5** Numerical model

**Table 1** Mechanical parameters of the rock strata

| Rock formation | Bulk modulus (GPa) | Shear modulus (GPa) | Density (kg m⁻³) | Friction angle (°) | Cohesion (MPa) | Tensile strength (MPa) |
|---|---|---|---|---|---|---|
| Sandy mudstone | 3.8 | 2.6 | 2350 | 32 | 3.3 | 2.4 |
| Fine sandstone | 11.3 | 6.8 | 2500 | 34 | 3.1 | 2.7 |
| Mudstone | 3.6 | 2.1 | 2300 | 32 | 2.3 | 2.2 |
| Sandstone | 9.2 | 3.2 | 2400 | 32 | 2.6 | 2.3 |
| Coal | 1.3 | 1.1 | 1600 | 28 | 1.8 | 0.75 |
| Siltstone | 13.3 | 10.8 | 2600 | 35 | 4.9 | 2.9 |

horizontal lateral pressure coefficients, and coal seam inclination angles. The influences of various conditions on the distribution characteristics of the stress deviator are analyzed.

## Numerical model

The mechanical parameters of the strata are shown in Table 1, the mechanical parameters of each rock layer in the model are derived from mechanical experiments with on-site rock samples. In addition, the numerical calculation model is shown in Fig. 5, and the distribution of rock strata in the model was based on the rock column chart in Fig. 1.

To obtain the rock parameters of each rock layer, we collected data from the mine and conducted triaxial and tensile tests on rock samples sampled on-site. The tensile strength is obtained by conducting a tensile test. The cohesion, friction angle, Poisson's ratio and Young's modulus of the rock are obtained conducting triaxial compression experiments. Furthermore, the bulk modulus ($K$) and shear modulus ($G$) of the rock are calculated based on Young's modulus ($E$) and Poisson's ratio ($\mu$). According to the knowledge of material mechanics, the specific calculation standards are formula (6) and formula (7):

$$K = \frac{E}{3(1 - 2\mu)} \tag{6}$$

$$G = \frac{E}{2(1 + \mu)}. \tag{7}$$

The model size is $x \times y \times z = 200\,\text{m} \times 20\,\text{m} \times 50\,\text{m}$ (in the numerical model, $x$ is the horizontal direction, and $z$ is the vertical direction), and $0 \leq x \leq 90$ for the #02 coal seam is the 10606 longwall panel. The horizontal displacements in the $x$ and $y$ directions of the model boundary are restricted, and the vertical displacement in the $z$ direction at the bottom of the model is restricted. Multiple sets of stress $P$ (load applied to the top of the model), lateral pressure coefficients $\lambda$ and coal seam inclination angles $\theta$ are selected for numerical calculation. The calculation adopts the Mohr–Coulomb strength criterion. The stress deviator distribution map of the surrounding rock is drawn by postprocessing the calculated results for the model.

## Distribution characteristics of the stress deviator for different *H* values

The area of the entire coalfield reaches approximately 2000 square kilometers. The surface of the coalfield is full of hills and ravines, so the burial depth of some panels can reach 200–600 m. According to the in situ stress data of the Malan Mine, the vertical and horizontal stresses near the 10606
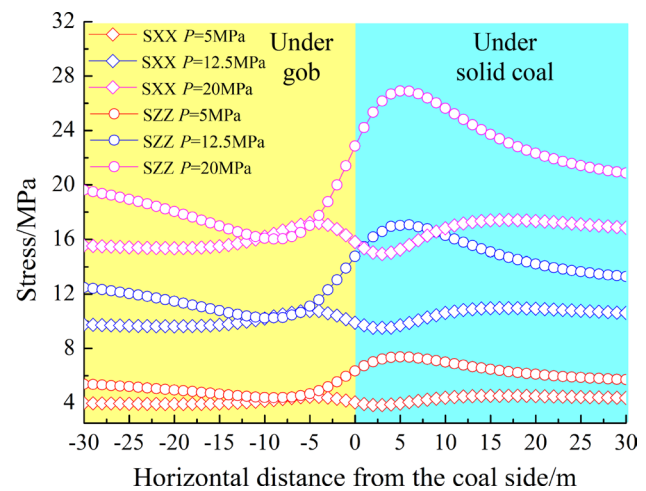
**Fig. 6** Stress distribution after excavation of a 10606 panel (different *P*)

panel are approximately 10 MPa and 8 MPa, respectively, and $\lambda$ is 0.8.

As the depth of the coal seam changes, the surrounding rock environment (including temperature and joints, etc.) will also change. However, the most important change is that with the increase in the thickness of the coal seam overlying rock, the stress environment of the surrounding rock changes accordingly. During numerical calculation, this section changes the stress conditions to simulate the stress environment of the surrounding rock under different burial depths.

To study the influence of coal seam depth on the distribution characteristics of the stress deviator in the rock surrounding the gob, the coal seam inclination angle and horizontal lateral pressure coefficient of the numerical model are set to $\theta = 0°$ and $\lambda = 0.8$, respectively. Uniform loads ($P$) of 5 MPa, 7.5 MPa, 10 MPa, 12.5 MPa, 15 MPa, 17.5 MPa and 20 MPa are applied to the top of the model.

Since the choice of the roadway location is located in the #2 coal seam, when the model under different stress states excavated 10606 panels and calculated the balance, we extracted the residual stress at the #2 coal seam, as shown in Fig. 6. Due to space limitations, stress distribution maps for $P = 5$ MPa, 12.5 MPa and 20 MPa are selected. As shown in Fig. 6, the horizontal residual stress (SXX) in the rock changes slightly with the horizontal position. The vertical residual stress (SZZ) changes drastically near the coal side; this change will lead to an increase in stress deviator. In addition, as $P$ increases, both SXX and SZZ in the surrounding rock show linear growth.

As shown in Fig. 7, to illustrate the influence of $P$ on the distribution characteristics of the stress deviator more intuitively, the same display gradient is selected when drawing the stress deviator distribution map under different conditions. In the figure, $-20 \leq x \leq 0$ is the
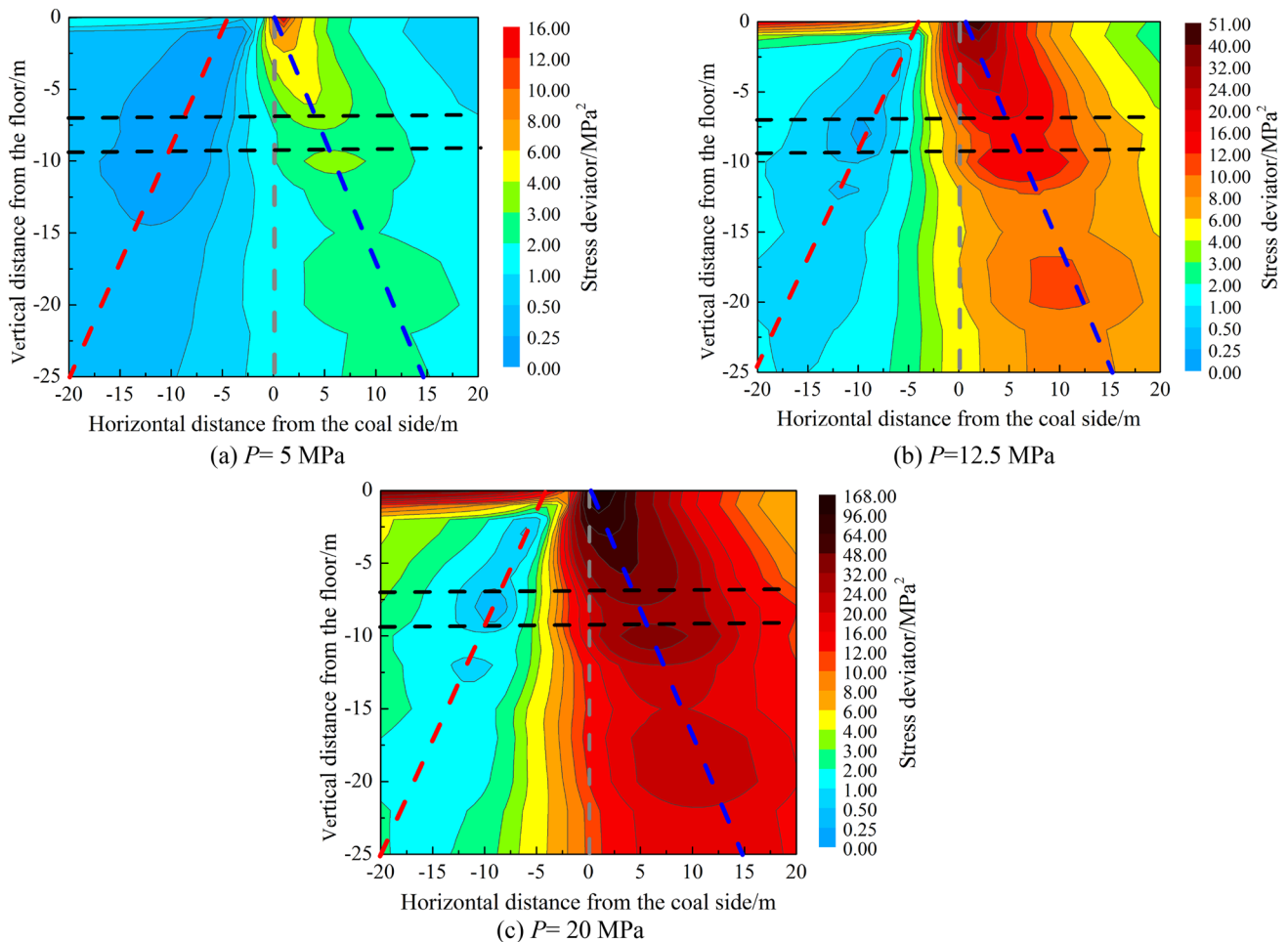
**Fig. 7** Influence of *P* on the distribution characteristics of the stress deviator

surrounding rock below the gob, and $0 \leq x \leq 20$ is the surrounding rock below the solid coal. In the figure, the gray dotted line represents $x = 0$, and the black dotted lines represent the roof and floor of the #2 coal seam. The blue dotted line represents the corresponding position of the maximum stress deviator at each depth (stress deviator peak axis), and the red dashed line represents the corresponding position of the minimum stress deviator at each depth (stress deviator valley axis).

As shown in Fig. 7, when $\theta = 0°$ and $\lambda = 0.8$, the stress deviator concentration area is below the solid coal, and the stress deviator release area is below the gob. The stress deviator in the rock mass below the coal side changes dramatically with the horizontal position. The distribution of stress deviator generally shows a trend of gradually decreasing with $z$.

Comparing Fig. 7a, b, and c, as $P$ increases, the value of the stress deviator increases significantly, and the stress deviator concentration area increases significantly, while the

distribution position of the stress deviator concentration area does not obviously change. The angle between the peak axis of the stress deviator and the vertical direction is always approximately 30°, and the angle between the axis of the minimum stress deviator and the vertical direction is always approximately -35°.

In Fig. 8a, b, c, the stress deviator curves at depths of $z = 0$ m, $-10$ m and $-20$ m under the gob are selected. The stress deviator curves of the rock masses at various depths generally present "single peak" distributions, and the peak position remains basically unchanged when the depth of the mining coal seam changes. The stress deviator is low under the gob, increases rapidly under the coal side, and quickly decreases after reaching a peak under the solid coal.

Taking $P = 20$ MPa as an example, when the $z$ values are 0 m, $-10$ m, and $-20$ m, the maximum stress deviator are 167.80, 36.95, and 23.84 MPa$^2$, respectively; and the corresponding peak positions are $x = 1$ m, 6 m, and 10 m, respectively. As $z$ increases, the peak stress deviator
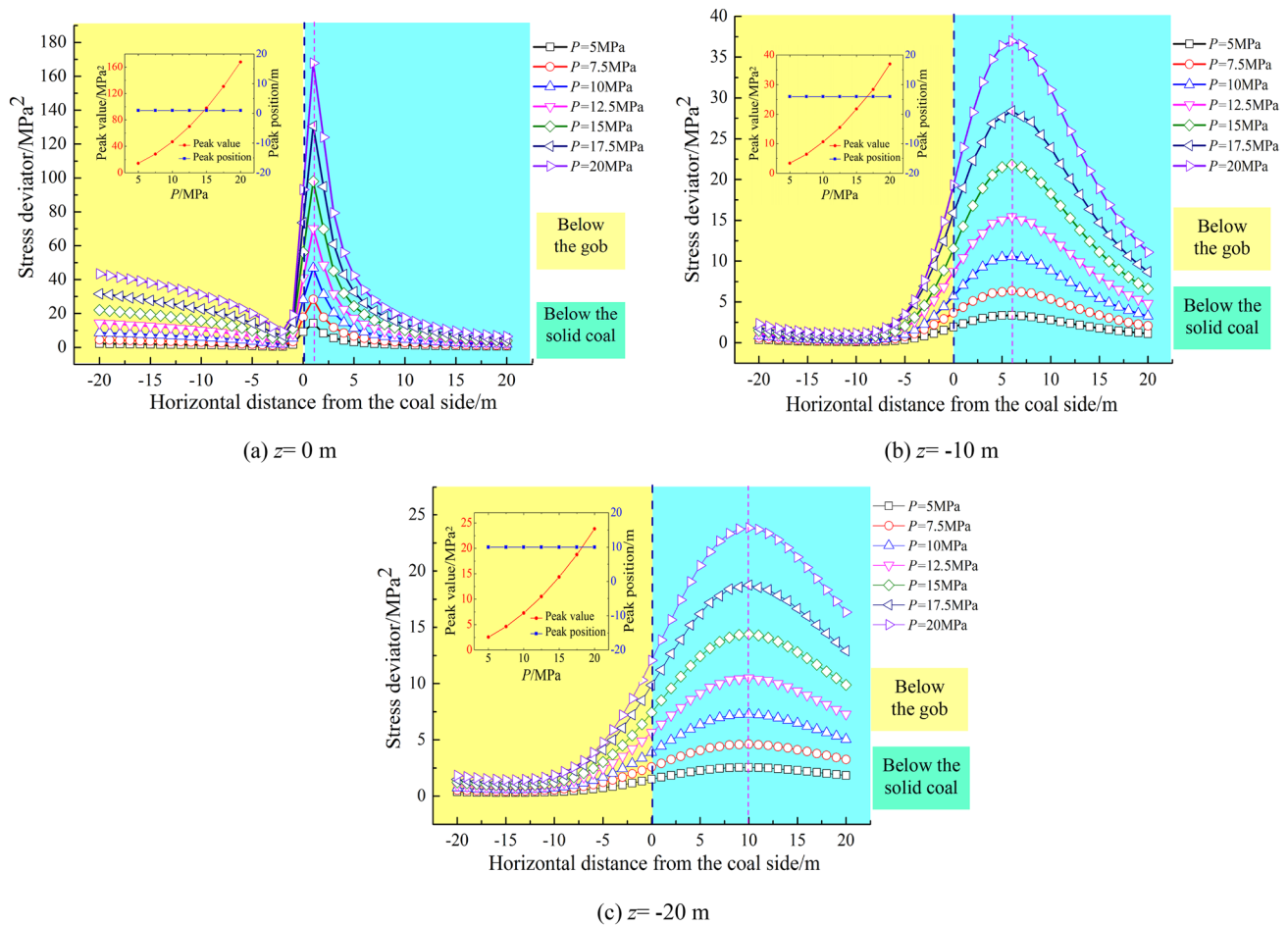
(a) $z= 0$ m

(b) $z= -10$ m

(c) $z= -20$ m

**Fig. 8** Distribution characteristics of the stress for different $P$ values

and the rate of change decrease, and the peak position gradually moves away from the coal side ($x = 0$).

Taking Fig. 8c as an example, when $P = 5$ MPa, 10 MPa, 15 MPa and 20 MPa, the maximum stress deviator in the surrounding rock are 2.55, 7.28, 14.38 and 23.84 MPa², respectively. As $P$ and $H$ increase, the rock mass stress deviator has a significant nonlinear increase, and the greater $P$ and $H$ are, the faster the growth rate of the stress deviator. These results indicate that in deep mining, the stress deviator in the rock surrounding the gob is greater, the distortion energy density is greater, and the risk is higher.

## Distribution characteristics of the stress deviator for different λ values

Affected by geological structures (such as faults, anticlines, synclines) and other factors, the horizontal pressure coefficients at different panels of the coal field are not exactly

the same. To study the influence of different lateral pressure coefficients $\lambda$ on the distribution characteristics of the stress deviator in the surrounding rock, a numerical calculation model was set up for a mining coal seam depth of 400 m and a coal seam inclination angle $\theta = 0°$; a uniform load of 10 MPa was applied to the top of the model. The horizontal lateral pressure coefficients were selected as $\lambda = 0.5$, $\lambda = 0.8$, $\lambda = 1.0$, $\lambda = 1.2$ and $\lambda = 1.5$.

Figure 9 shows the residual stress at the #2 coal seam after excavating 10606 panels and calculating the balance of the numerical model under different $\lambda$. As shown in Fig. 9, when $\lambda$ is different, the residual stress in the vertical direction (SZZ) below the gob floor is basically the same, but the residual stress in the horizontal direction (SXX) below the gob is quite different, and the stress will increase linearly with the increase in $\lambda$. This phenomenon will lead to changes in the distribution range of the stress deviator concentration area.
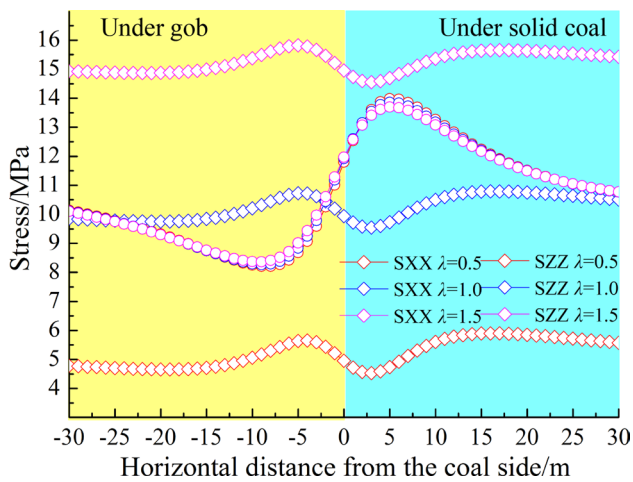
**Fig. 9** Stress distribution after excavation of a 10606 panel (different λ)

Figure 10a,b,c shows the stress deviator distribution diagrams when λ is 0.5, 1.0 and 1.5. The diagrams illustrate that the location of the stress deviator concentration area in the surrounding rock below the gob changes with the change in λ. When λ = 0.5, the stress deviator concentration area in the floor is located under the solid coal. The peak stress deviator axis and the vertical direction are at an angle of approximately 30°, and the minimum stress deviator axis is at an angle of -35° from the vertical direction. When λ = 1.5, the stress deviator concentration area is located below the gob, the peak axis of the stress deviator is at an angle of approximately -45° from the vertical direction, and the minimum axis of the stress deviator is at an angle of approximately 27° from the vertical direction. When λ = 1.0, the distribution of the stress deviator is more uniform, and the values of the stress deviator are generally low.

As shown in Fig. 11a,b,c, the stress deviator concentration area in the lower shallow part ($z = 0$) below the gob is near the coal side. When $λ ≤ 1.0$, the position of the peak stress deviator moves in the positive $x$ direction, and when $λ > 1.0$, the position of the peak stress deviator moves in the negative $x$ direction.

Taking Fig. 11c as an example, at 20 m below the gob, when the λ values are 0.5, 0.8, 1.0, 1.2 and 1.5, the maximum stress deviator are 19.65, 7.28, 2.42, 2.94 and 11.78 $MPa^2$, respectively. These results show that the greater
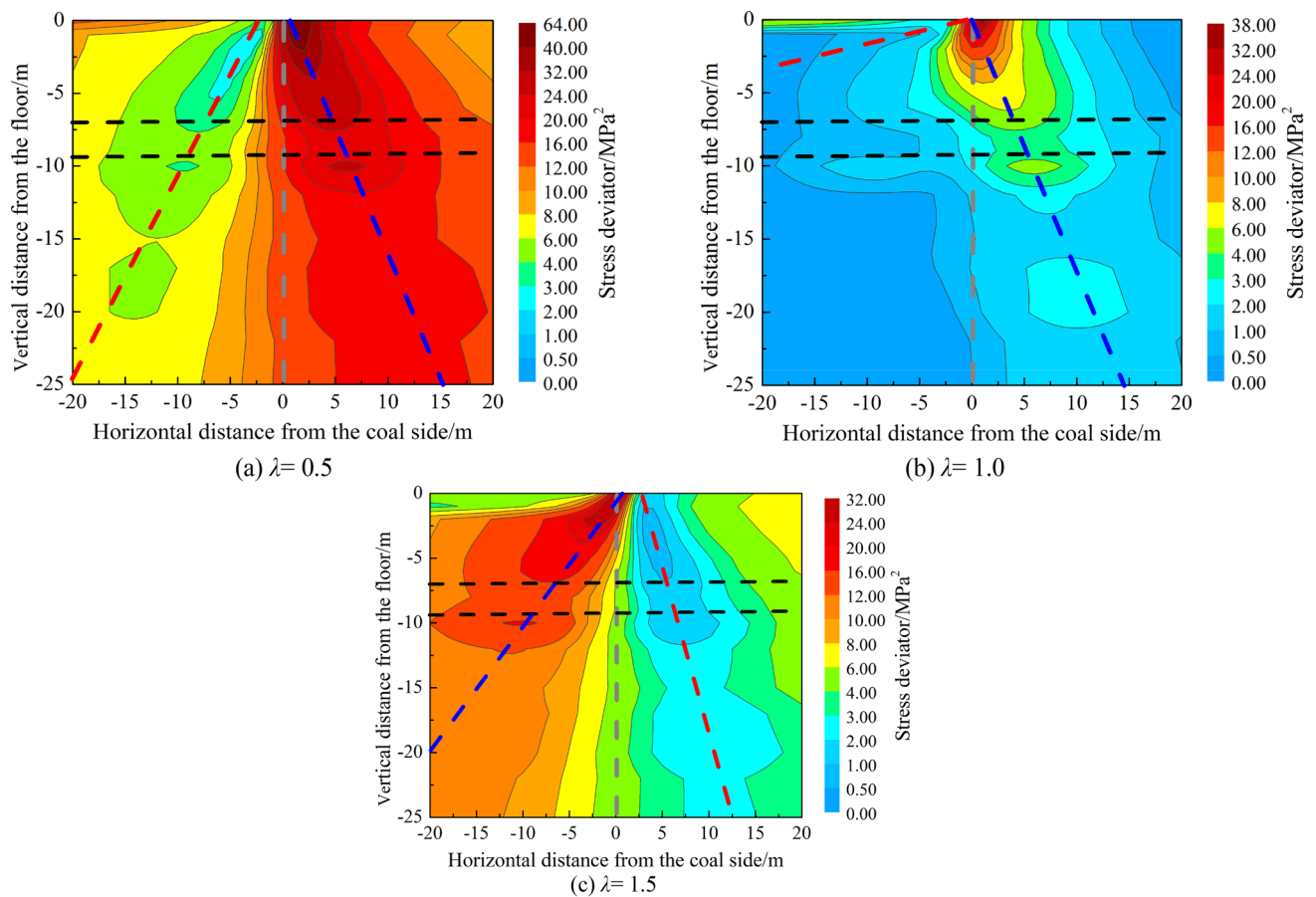


(a) λ = 0.5



(b) λ = 1.0



(c) λ = 1.5

**Fig. 10** Influence of λ on the distribution characteristics of the stress deviator

(a) $z$= 0 m



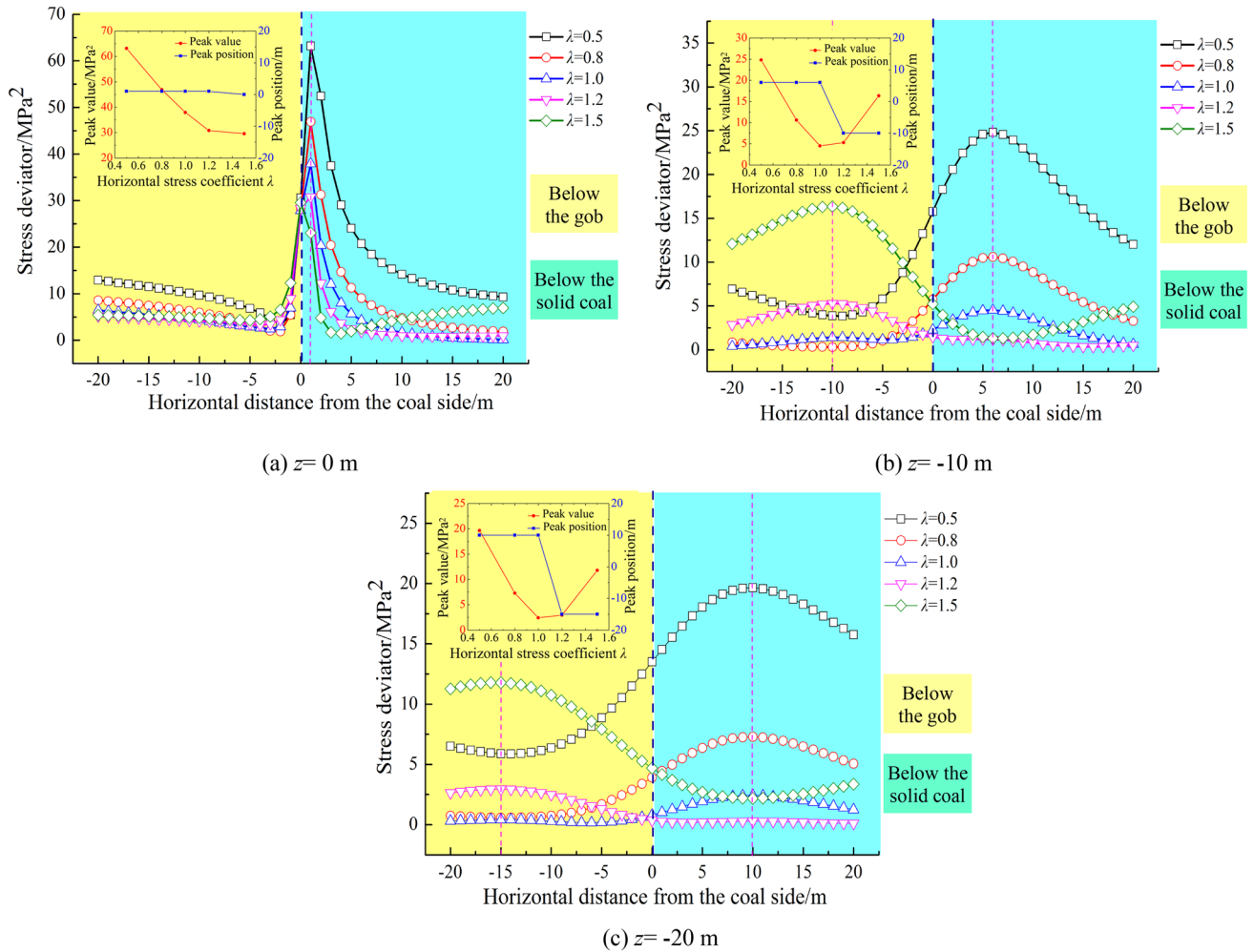(b) $z$= -10 m



(c) $z$= -20 m

**Fig. 11** Distribution characteristics of the stress deviator for different $\lambda$ values

the difference between $\lambda$ and 1.0 is, the greater the stress deviator. When the $\lambda$ values are 0.5, 0.8, and 1.0, the corresponding peak position is $x$ = -15 m; when the $\lambda$ values are 1.2 and 1.5, the corresponding peak position is $x$ = 10 m. These results indicate that $\lambda$ directly affects the position of the stress deviator concentration area and the size of the stress deviator.

## Distribution characteristics of the stress deviator for different $\theta$ values

The exploitation of inclined coal seams is very common in mining engineering. To study the influence of the coal seam inclination angle on the distribution characteristics of the stress deviator in the surrounding rock, the numerical calculation model is set to $\lambda$ = 0.8, and a uniform load of 10 MPa is applied to the top of the model. In this paper, a counterclockwise rotation angle of the horizontal coal seam is

recorded as "+", and a clockwise rotation angle is recorded as "−". The coal seam inclination angles for the model are selected as $\theta = -30°$, $\theta = -15°$, $\theta = 0°$, $\theta = 15°$, and $\theta = 30°$.

Figure 12 shows the residual stress at the #2 coal seam after excavating 10606 panels and calculating the balance of the numerical model under different $\theta$. As shown in Fig. 12, with the increase in $\theta$, the vertical residual stress (SZZ) under the gob floor also increases, while the horizontal residual stress (SXX) under the gob floor shows fluctuating changes, but the degree of change is smaller than that of SZZ; these changes will lead to changes in the magnitude and distribution of the stress deviator under the gob floor.

Figure 13a,b,c shows the stress deviator distribution when $\theta$ is -30°, 0° and 30°. In the figure, the $x$-axis is the horizontal direction of the model, and the $y$-axis is the vertical direction of the model. When $\theta = -30°$, $\theta = 0°$, and $\theta = 30°$, the angle between the peak axis of the stress deviator and the vertical direction has values of approximately 22°, 26°,
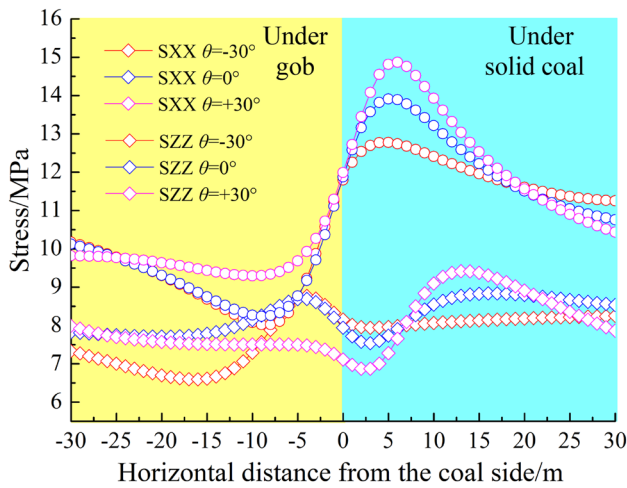
Fig. 12 Stress distribution after excavation of a 10606 panel (different $\theta$)

and 39°, respectively. Taking (0,0) as the origin coordinates in the figure, the stress deviator concentration area rotates

counterclockwise in the same direction as the change in $\theta$, and the rotation angle of the stress deviator concentration area is smaller than $\theta$. In addition, as $\theta$ increases, the stress deviator concentration area gradually increases, and the stress deviator value increases slightly.

In Fig. 14, the change curves of the rock mass stress deviator at 0 m, 10 m and 20 m below the gob are selected. The changes in the stress deviator curve maintain a relatively stable state in the surrounding rock below the gob, and the stress deviator increases rapidly and reaches a peak value near the coal side. Comparing Fig. 14a, b, and c and taking $\theta = 0°$ as an example, as $z$ increases, the peak values of the stress deviator are 46.92, 10.60 and 7.28 MPa$^2$, and the peak positions are $x = 1$ m, $x = 6$ m and $x = 10$ m, respectively. These results show that as $z$ increases, the stress deviator value and the rate of stress deviator change gradually decrease.

Taking Fig. 14c as an example, when the $\theta$ values are -30°, -15°, 0°, 15°, and 30°, the peak values of the stress deviator are 5.06, 6.51, 7.28, 6.70, and 10.52 MPa$^2$, respectively. The coordinate positions corresponding to



(a) $\theta = -30°$



(b) $\theta = 0°$



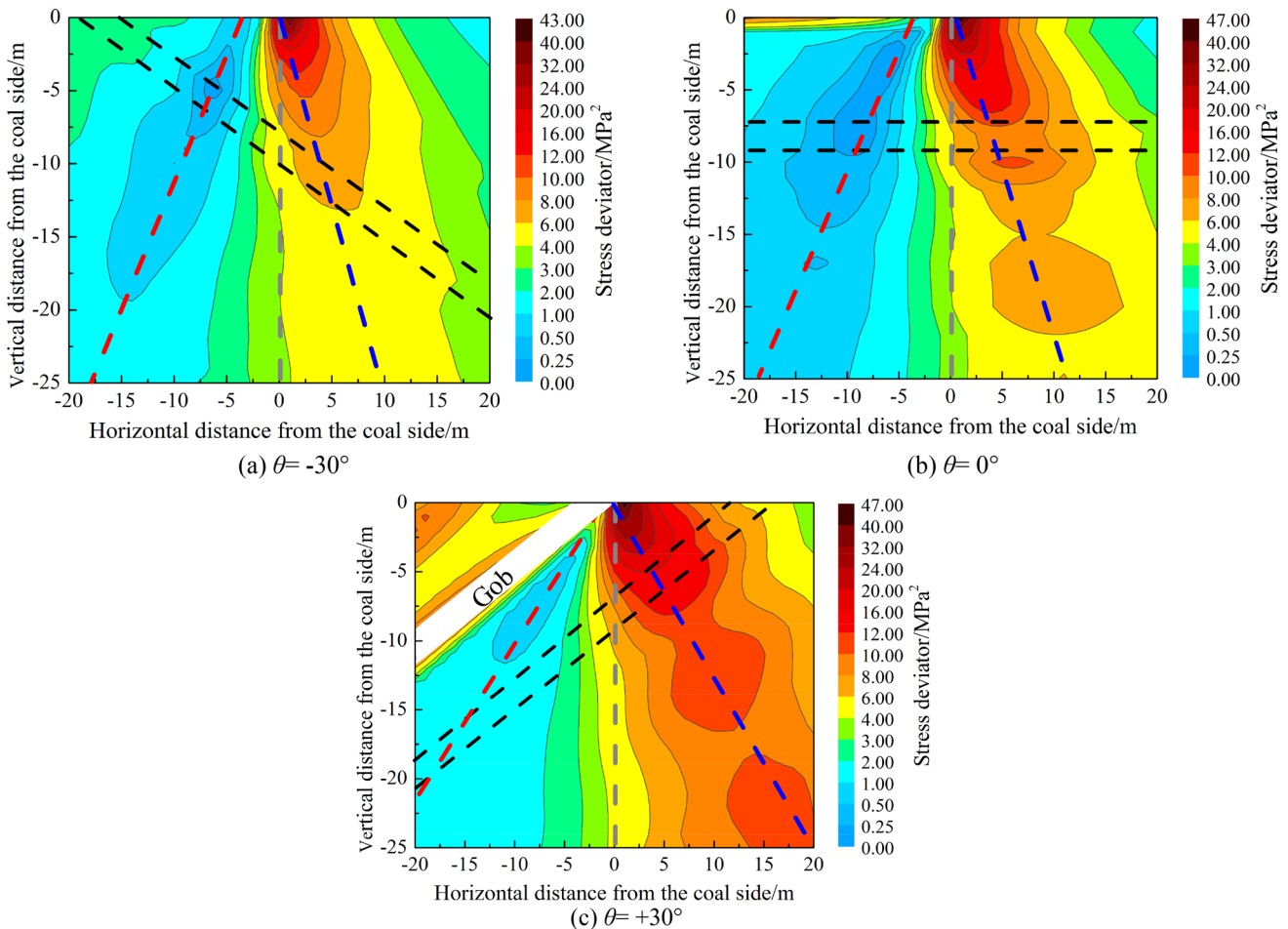(c) $\theta = +30°$

Fig. 13 Influence of $\theta$ on the distribution characteristics of the stress deviator
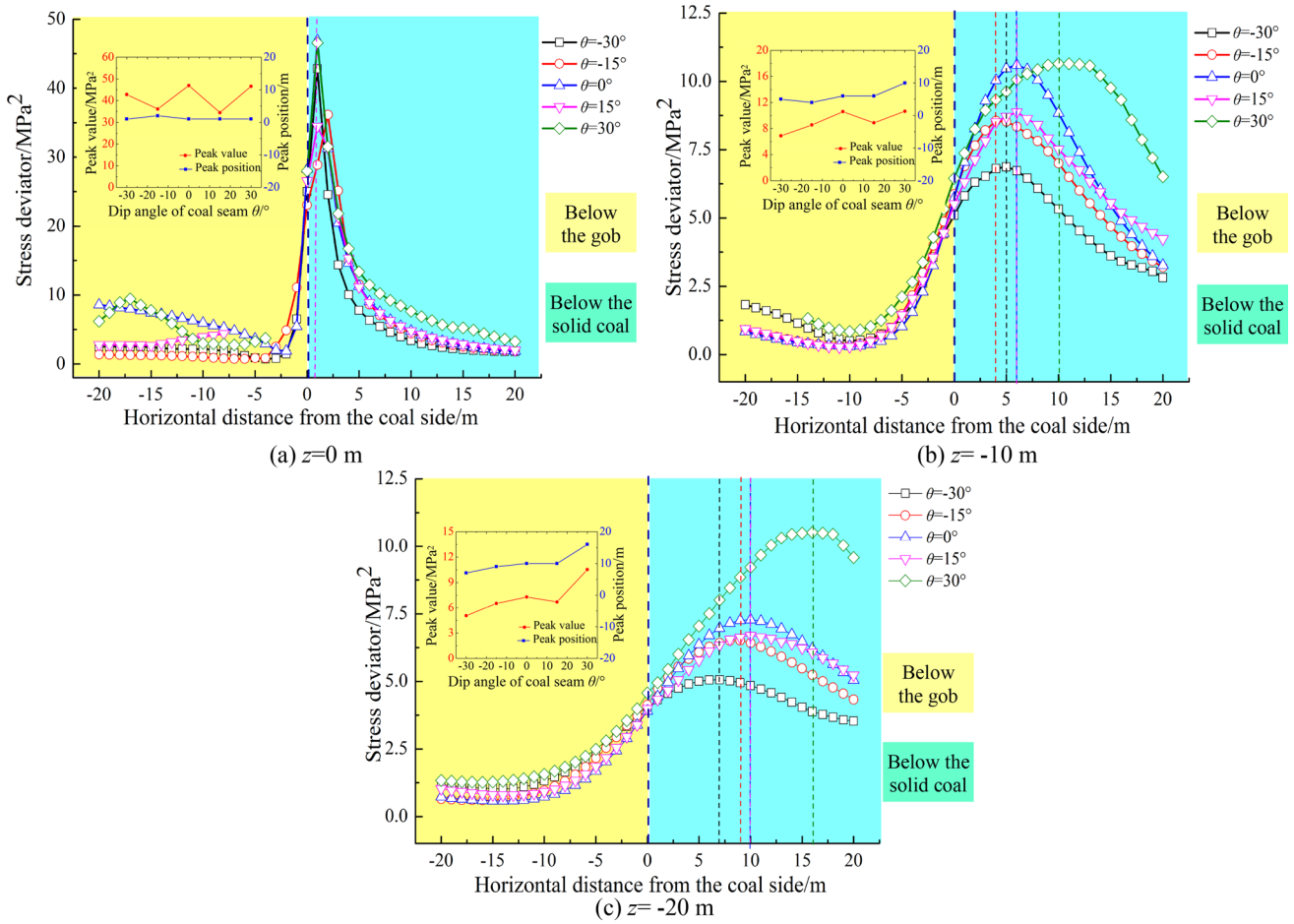
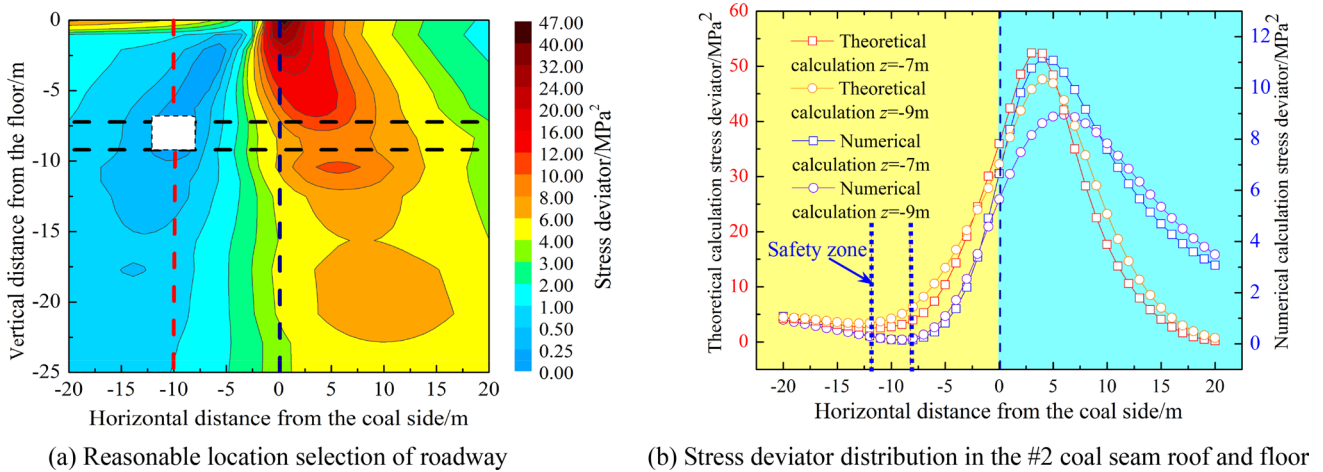Fig. 14 Distribution characteristics of the stress deviator for different $\theta$ values



(a) Reasonable location selection of roadway

(b) Stress deviator distribution in the #2 coal seam roof and floor

Fig. 15 Stress deviator distribution and reasonable location selection of roadway

the peak values are $x = 7$ m, $x = 9$ m, $x = 10$ m, $x = 10$ m and $x = 16$ m. This finding indicates that with the increase in $\theta$, the stress deviator in the surrounding rock below the gob generally shows a slight increasing trend, while the locations of the peak values and the stress deviator concentration area gradually move away from the gob. Therefore, $\theta$ has a relatively small influence on the stress deviator but obviously affects the distribution of the stress deviator concentration area.

## Discussion

### Primary selection of a reasonable location for the roadway

During the mining of the closely spaced coal seams in the Malan Mine, the #2 coal seam is located 7 m–9 m below the floor of the #02 coal seam. The burial depth of the 10606 panel is approximately 400 m, and the inclination angle of the coal seam is almost horizontal. According to the crustal stress data, the horizontal lateral pressure coefficient $\lambda = 0.8$. Therefore, according to the mine data, $H = 400$ m, $\theta = 0°$, $\lambda = 0.8$, $K = 2.4$, $l = 21.8$ m, $m = 2$ m, and $n = 15$ m are substituted into formulas (1), (2), (3), and (5) to obtain the theoretical calculated results for the stress deviator.

Similarly, Fig. 15 shows the results of the theoretical calculations and numerical simulations of the stress deviator at 7 m and 9 m below the gob (Fig. 15b) when the in situ stress parameters of the 10606 panel are substituted into the numerical simulation. 7 m and 9 m below the gob are the positions of the roof and floor, respectively, for the #2 coal seam (the black dotted line in Fig. 15a).

As shown in Fig. 15, the changes in the stress deviator for the theoretical calculation are basically consistent with those for the numerical calculation. Below the solid coal, 3–5 m away from the coal side ($x = 0$), the stress deviator reaches its peak value and decreases rapidly with increasing horizontal distance from the gob. Below the gob, the stress deviator decreases rapidly as the distance between the surrounding rock and the coal side ($x = 0$) increases. After reaching a minimum value, as the distance from the coal side ($x = 0$) continues to increase, the stress deviator increases slightly. In the range of -12 m $\leq x \leq$ -8 m, the results of the theoretical calculation and the numerical calculation both reach a minimum, and the rate of change in the stress deviator is very low, thus indicating that the distortion energy density in the rock mass is low in this range and that the stability of the surrounding rock is good, thus, this position for the #2 coal seam gas drainage roadway is suitable (Fig. 15a).
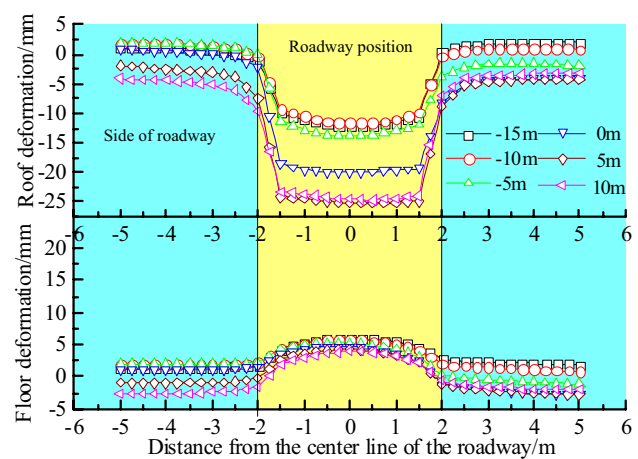


**(a)** Deformation of roadway roof and floor at various positions
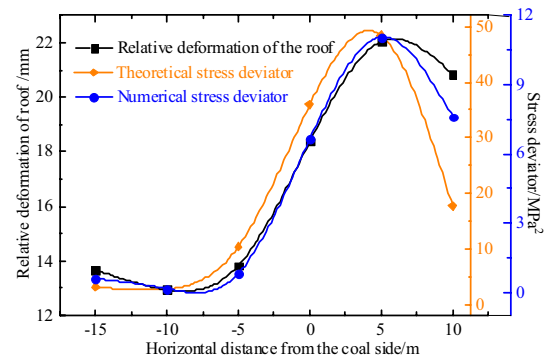


**(b)** Stress deviator and relative deformation of roof

**Fig. 16** Rationality analysis of roadway position

### Verification of the reasonable location for the roadway

To verify the rationality of the abovementioned location of the gas drainage roadway in #2 coal seam, in the numerical calculation, after the formation of the 10606 gob, 6 sets of comparative simulations were carried out on the excavation of the gas drainage roadway in #2 coal seam. In the comparative simulation, the horizontal distances between the roadway and coal side are $-15$ m, $-10$ m, $-5$ m, 0 m, $+5$ m and $+10$ m, respectively. The cross section of the roadway is rectangular, and the size is width (4.0 m) × height (2.5 m).

The study found that the maximum deformation of the roadway is located on the roof and floor of the roadway, and the roof and floor deformation data of the roadway at various locations are extracted, as shown in Fig. 16a. Figure 16a shows that the roof deformation of the roadway is obviously greater than that of the floor, and when the excavation position of the roadway is at $x = -10$ m, the deformation of the roof is the smallest, followed by $x = -15$ m and $x = -5$ m.
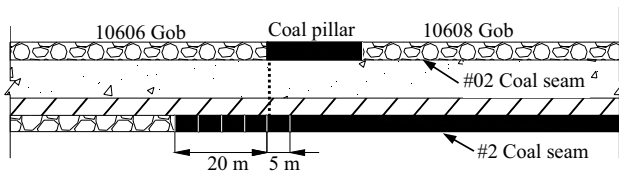
**Fig. 17** Excavation boundary position of the lower coal seam in the numerical simulation

At the same time, it can be seen that there are also some surrounding rock deformations caused by the mining of the upper coal seam far away from the roadway, which leads to different starting positions of the deformation curves in Fig. 16a. Therefore, we take the deformation at the centerline of the roadway minus the average value of the deformation at -5 m and +5 m from the centerline of the roadway as the relative deformation of the roof.

The relative deformation curve of the roadway and the stress deviator curve obtained by theoretical calculation and numerical simulation are shown in Fig. 16b for comparison. The results show that the deformation of the roadway has the same changing law as the stress deviator. As $x$ increases, it first decreases slowly, reaches the minimum when $x = -10$ m, then rises rapidly (below the coal side), reaches the maximum value at $x = +5$ m, and then decreases slowly. At $x = -10$ m, the minimum relative deformation is 12.95 mm. This result shows that when excavating a roadway at $-8$ to $-12$ m, the stress deviator, distortion energy density and deformation are small, and the state of the surrounding rock is relatively stable.

## Verification of the reasonable position of the panel boundary

The gas drainage roadway not only provides gas drainage services for multiple other longwall panels but also serves as the mining roadway for the #2 coal seam. Therefore, the location of the gas drainage roadway is the boundary position of the longwall panel for the #2 coal seam. Hence, it is not enough to consider only the stability of the roadway when designing a reasonable arrangement of the roadway. Considering the stability of the surrounding rock of the entire mining area during the mining of the #2 coal seam after the #02 coal seam is mined is also important.

In this section, the numerical model is simulated in accordance with the on-site mining sequence. After the model has successively completed the mining of the 10606 and 10608 longwall panels of the #02 coal seam, the 20 m protective coal pillar is retained, and mining of the #2 coal seam (the lower coal seam) is started after the model calculates the balance (Fig. 18a).

In the process of mining the #2 coal seam, the stress deviator distributions of the surrounding rock when the boundary of the longwall panel of the #2 coal seam is at horizontal distances $x = -20$ m, $-15$ m, $-10$ m, $-5$ m, 0 m and $+5$ m from the edge of the coal pillar are studied. The excavation boundary position of the lower coal seam in the numerical simulation is shown in Fig. 17.

This section selects the stress deviator distributions when $x = -20$ m, $-10$ m, 0 m and $+5$ m for analysis.

As shown in Fig. 18, when the horizontal distance between the boundary of the #2 coal seam and the edge of the coal pillar is $x < 0$, $x > 0$, and $x = 0$, the #2 coal seam mining area forms an internal staggered arrangement, an external staggered arrangement, and an overlapping arrangement, respectively.

The figure shows that when $x = -20$ m (Fig. 18b), the stress deviator in the rock mass below the coal pillar ($0 \leq x \leq 20$) is evenly distributed, and the maximum stress deviator at the two edges of the coal pillar are 55.85 and 46.06 MPa$^2$. The #2 coal seam has an obvious stress deviator concentration at the boundary of the longwall panel, and the maximum stress deviator is 58.96 MPa$^2$; when $x = -10$ m (Fig. 18c), the stress deviator on both sides of the coal pillar are 68.09 and 46.90 MPa$^2$, and the maximum stress deviator at the #2 coal seam is 45.66 MPa$^2$; when $x = 0$ m (Fig. 18d), The panels are overlapping arrangement, and the stress deviator of the surrounding rock under the coal pillar ($0 \leq x \leq 20$) increases rapidly. The stress deviator on two sides of the coal pillar are 65.93 and 52.40 MPa$^2$. The maximum stress deviator in the #2 coal seam is 80.62 MPa$^2$; when $x = +5$ m (Fig. 18e), the panels are external staggered arrangement. Due to the stress unloading of the #02 coal seam, the stress deviator are all concentrated in the #2 coal seam, and the maximum stress deviator of the #2 coal seam reaches 115.78 MPa$^2$.

These results show that as when $x < 0$, the horizontal distance between the panel boundary of the #2 coal seam and the edge of the coal pillar gradually decreases, the stress deviator in the surrounding rock of the coal pillar gradually increases, and the stress deviator of the surrounding rock near the 10606 panel boundary increases more obviously. The stress deviator at the panel boundary of the #2 coal seam first decreases and then increases rapidly.

To more intuitively display the changes in the stress deviator in the surrounding rock during mining of the #2 coal seam, the stress deviator values of the #02 coal seam floor and the #2 coal seam floor when the $x$ values differ are extracted, as shown in Fig. 19.

According to Fig. 19a, due to the mining of the #2 coal seam, an asymmetrical distribution of stress deviator appears under the coal pillar of the #02 coal seam.
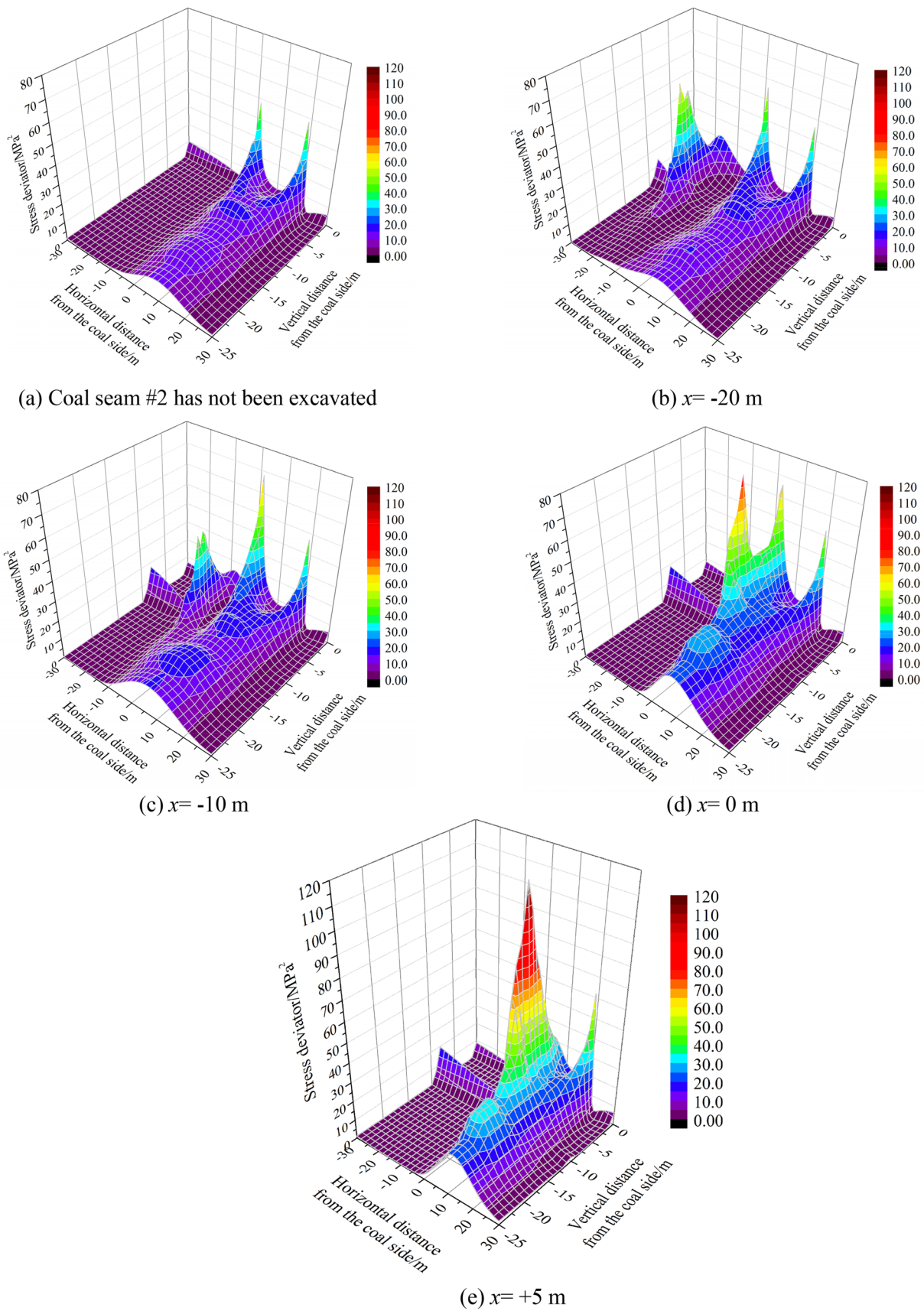
(a) Coal seam #2 has not been excavated

(b) x= -20 m

(c) x= -10 m

(d) x= 0 m

(e) x= +5 m

**Fig. 18** Stress deviator distribution during #2 coal seam mining

(a) Stress deviator distribution in the #02 coal seam floor ($z$=0)



(b) Stress deviator distribution in the #2 coal seam floor ($z$= -9)
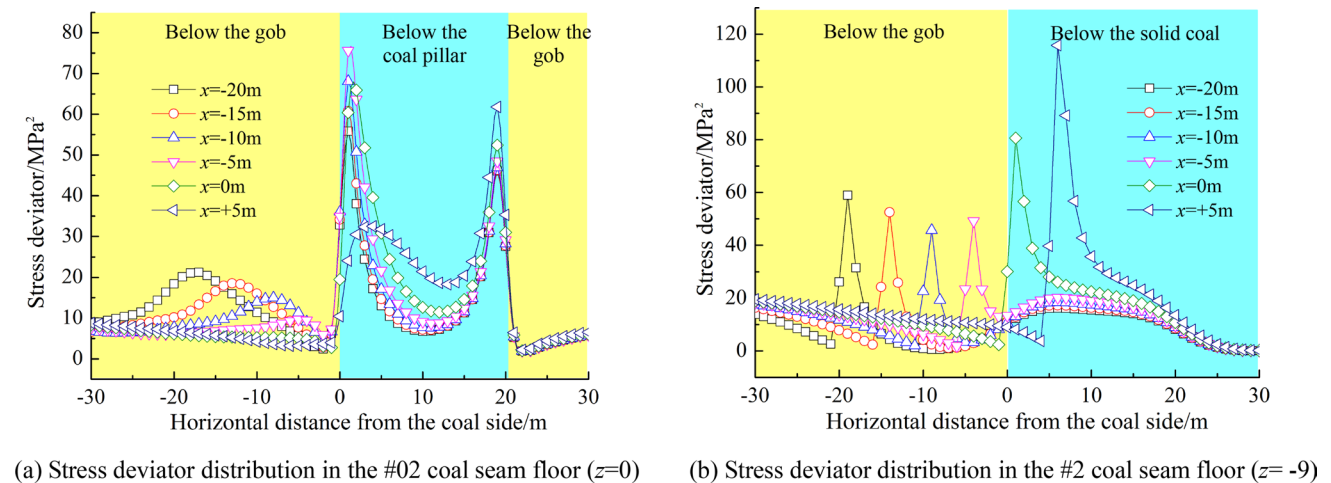
**Fig. 19** Patterns of stress deviator changes during mining of the #2 coal seam

When $x > 0$, mining the #2 coal seam causes vertical stress unloading on one side of the coal pillar of the #02 coal seam, and the stress deviator in the floor of the #02 coal seam decreases significantly, but at this time, the stress deviator in the floor of the #2 coal seam rises sharply (Fig. 19b). When $x = +5$ m, the maximum stress deviator of the #2 coal seam floor reaches 115.78 MPa². At this time, the stability of the rock mass in the #2 coal seam is poor. Therefore, positioning the roadway at $x > 0$ (an external staggered arrangement) is not recommended.

When $x < 0$, with changes in $x$, the peak stress deviator in the #02 coal seam floor changes slightly, and the stress deviator peak in the #2 coal seam floor first decreases and then increases. When $x = -10$ m, the peak stress deviator is the lowest, and the minimum is 45.66 MPa². Therefore, from the perspective of the stress deviator distribution and surrounding rock stability after mining the #2 coal seam, the mining boundary of the #2 coal seam should be within the range -15 m $< x <$ -5 m.

Based on the above analysis, combining the distribution of the stress deviator in the surrounding rock under a single gob during the roadway excavation and the distribution of the stress deviator in the surrounding rock after the #2 coal seam is mined shows that the best location for laying out the gas drainage lower roadway is located -8 ~ -12 m from the edge of the reserved coal pillar in the #2 coal seam (Fig. 15a).

Most previous studies used experience or vertical stress to select the location of the roadway layout without considering the stress deviator. However, mining coal seams will lead to the plastic failure of the floor. The surrounding rocks in some roadway locations have undergone serious plastic failure

before excavation; such failure makes roadway excavation and support very difficult. Some scholars have studied the elasto-plastic state of the surrounding rock by calculating and analyzing the stress deviator, thereby ensuring the stability of the surrounding rock at the location of the new roadway (Sun et al 2016; Xu et al 2015), and have successfully solved how to determine a reasonable location for the roadway (Xu 2014; Zhou et al 2016).

In future research, the stress deviator should be used as an important parameter for studying the stability of the surrounding rock. There are still some shortcomings in the research presented in this paper. For example, the scheme has not been applied and verified on-site due to the impact of the construction period and other reasons. In addition, the geological conditions considered in this study are relatively simple, and the influence of factors, such as groundwater (Ma et al. 2017) and complex geological structures (Sainoki and Mitri 2016) has not been considered. This paper studies several factors that have macroscopic impacts on the stress deviator; however, faults (Li et al 2021; Zhu et al. 2017a, b) and other geological structures are very common in mining engineering. As the depth of coal seams increases, the environmental temperature, fractures, and bedding in the surrounding rock will increase. These factors will all affect the stress state. Structures, such as faults, fractures and bedding, will "block" the transfer of stress in the rock mass. The direction and magnitude of stress at the faults, fractures and bedding will change. Therefore, the surrounding rock stress near faults, fractures and bedding differs from the stress in a homogeneous rock mass. When there are some geological structures, the stress distribution is very complicated. The magnitude and distribution of the stress deviator near the structure are also affected by the width, inclination,

and stiffness of faults, fractures and bedding, which need to be further studied.

## Conclusions

1. Theoretical calculations yield the vertical, horizontal and shear stress formulas under a single inclined gob. Combining the calculation formulas for stress and $J_2$, the distributions of the stress deviator in the roof and floor of the #2 coal seam under a single gob in the Malan Mine are calculated, and the main factors that affect the distribution of stress deviator are obtained by the formulas; these factors are the coal seam depth $H$, horizontal pressure coefficient $\lambda$, and coal seam inclination angle $\theta$.

2. By postprocessing the numerical simulation calculation results, the distribution of the stress deviator under a single gob is obtained. The research results show that as $P\ (H)$ increases, the rock mass stress deviator has a nolinear increase, and the greater the $P$ value is, the faster the stress deviator growth rate. $\lambda$ directly affects the position of the stress deviator concentration area and the size of the stress deviator. $\theta$ has a relatively small influence on the size of the stress deviator but obviously affects the position of the stress deviator concentration area.

3. Analyzing the distributions of the stress deviator calculated by theoretical and numerical simulations gives a reasonable position for the gas drainage roadway in the Malan Mine. By studying the distribution of the stress deviator in the surrounding rock during the mining of the #2 coal seam, the stress deviator in the upper coal floor is found to be released when $x > 0$, and the stress deviator in the lower coal floor increases sharply. When $x < 0$, as the mining boundary of the lower coal seam gradually approaches the coal pillar of the upper coal seam, the stress deviator on both sides of the coal pillar changes slightly, and the stress deviator at the mining boundary of the lower coal seam first decreases and then increases. Finally, the rationality of the roadway layout is verified by the stability of the surrounding rock after mining in the lower coal seam.

## Declarations

**Informed consent** Informed consent was obtained from all individual participants in this study.

## References

Aguado MBD, Nicieza CG (2007) Control and prevention of gas outbursts in coal mines, Riosa-Olloniego coalfield, Spain. Int J Coal Geol 69(4):253–266. https://doi.org/10.1016/j.coal.2006.05.004

Bai QS, Tu SH, Wang FT, Zhang XG, Tu HS, Yuan Y (2014) Observation and numerical analysis of the scope of fractured zones around gateroads under longwall influence. Rock Mech Rock Eng 47(5):1939–1950. https://doi.org/10.1007/s00603-013-0457-9

Brady BH, Brown ET (1993) Rock mechanics: for underground mining. Springer Science and Business Media, Berlin

Cao Y, He D, Glick DC (2001) Coal and gas outbursts in footwalls of reverse faults. Int J Coal Geol 48(1–2):47–63. https://doi.org/10.1016/S0166-5162(01)00037-4

Cheng XJ, Wen H, Xu YH, Fan SX, Ren SJ (2020) Environmental treatment technology for complex coalfield fire zone in a close distance coal seam: a case study. J Therm Anal Calorim. https://doi.org/10.1007/s10973-020-10302-z

Das AJ, Mandal PK, Paul PS, Sinha RK (2019) Generalised analytical models for the strength of the inclined as well as the flat coal pillars using rock mass failure criterion. Rock Mech Rock Eng 52(10):3921–3946. https://doi.org/10.1007/s00603-019-01788-7

Jiang B, Wang L, Lu Y, Gu S, Sun X (2015) Failure mechanism analysis and support design for deep composite soft rock roadway: a case study of the Yangcheng coal mine in China. Shock Vib. https://doi.org/10.1155/2015/452479

Kroon M, Faleskog J (2013) Numerical implementation of a J2 and J3 dependent plasticity model based on a spectral decomposition of the stress deviator. Comput Mech 52(5):1059–1070. https://doi.org/10.1007/s00466-013-0863-6

Li ZL, Dou LM, Cai W, Wang GF, Ding YL, Kong Y (2016) Roadway stagger layout for effective control of gob-side rock bursts in the longwall mining of a thick coal seam. Rock Mech Rock Eng 49(2):621–629. https://doi.org/10.1007/s00603-015-0746-6

Li ZL, Shan RL, Wang CH, Yuan HH, Wei YH (2020) Study on the distribution law of stress deviator below the floor of a goaf. Geomech Eng 21(3):301–313. https://doi.org/10.12989/gae.2020.21.3.301

Li ZL, Wang CH, Shan RL, Yuan HH, Zhao Y, Wei YH (2021) Study on the influence of the fault dip angle on the stress evolution and slip risk of normal faults in mining. Bull Eng Geol Environ. https://doi.org/10.1007/s10064-021-02149-x

Liu X, Li X, Pan W (2016) Analysis on the floor stress distribution and roadway position in the close distance coal seams. Arab J Geosci 9(2):83. https://doi.org/10.1007/s12517-015-2035-9

Ma L, Jin Z, Liang J, Sun H, Zhang D, Li P (2015) Simulation of water resource loss in short-distance coal seams disturbed by repeated mining. Environ Earth Sci 74(7):5653–5662. https://doi.org/10.1007/s12665-015-4581-6

Ma D, Rezania M, Yu HS, Bai HB (2017) Variations of hydraulic properties of granular sandstones during water inrush: effect of small particle migration. Eng Geol 217:61–70. https://doi.org/10.1016/j.enggeo.2016.12.006

Sainoki A, Mitri HS (2016) Dynamic modelling of fault slip induced by stress waves due to stope production blasts. Rock Mech Rock Eng 49(1):165–181. https://doi.org/10.1007/s00603-015-0721-2

Shabanimashcool M, Li CC (2012) Numerical modelling of longwall mining and stability analysis of the gates in a coal mine. Int J Rock Mech Min Sci 51:24–34. https://doi.org/10.1016/j.ijrmms.2012.02.002

Shang H, Ning J, Hu S, Yang S, Qiu P (2019) Field and numerical investigations of gateroad system failure under an irregular residual coal pillar in close distance coal seams. Energy Sci Eng 7(6):2720–2740. https://doi.org/10.1002/ese3.455

Suchowerska AM, Merifield RS, Carter JP (2013) Vertical stress changes in multi-seam mining under supercritical longwall panels. Int J Rock Mech Min Sci 61:306–320. https://doi.org/10.1016/j.ijrmms.2013.02.009

Suchowerska AM, Carter JP, Merifield RS (2014) Horizontal stress under supercritical longwall panels. Int J Rock Mech Min Sci 70:240–251

Sun YJ, Xie SR, Li SJ, Song BH, Huang X (2016) Reasonable location of roadway in coal pillar area under different layer located key blocks and its surrounding rock control. J China Univ Min Technol. https://doi.org/10.13247/j.cnki.jcumt.000550 (**in Chinese**)

Sun J, Wang L, Zhao G (2019) Stress Distribution and failure characteristics for workface floor of a tilted coal seam. KSCE J Civ Eng 23(9):3793–3806. https://doi.org/10.1007/s12205-019-0786-7

Tan YL, Zhao TB, Xiao YX (2010) In situ investigations of failure zone of floor strata in mining close distance coal seams. Int J Rock Mech Min Sci 47(5):865–870. https://doi.org/10.1016/j.ijrmms.2009.12.016

Tian M, Han L, Meng Q, Ma C, Zong Y, Mao P (2020) Physical model experiment of surrounding rock failure mechanism for the roadway under deviatoric pressure form mining disturbance. KSCE J Civ Eng. https://doi.org/10.1007/s12205-020-1540-x

Toraño J, Díez RR, Cid JR, Barciella MC (2002) FEM modeling of roadways driven in a fractured rock mass under a longwall influence. Comput Geotech 29(6):411–431. https://doi.org/10.1016/S0266-352X(02)00006-X

Wang FT, Zhang C, Wei SF, Zhang XG, Guo SH (2016) Whole section anchor–grouting reinforcement technology and its application in underground roadways with loose and fractured surrounding rock. Tunn Undergr Space Technol 51:133–143. https://doi.org/10.1016/j.tust.2015.10.029

Wang Q, Pan R, Jiang B, Li SC, He MC, Sun HB (2017) Study on failure mechanism of roadway with soft rock in deep coal mine and confined concrete support system. Eng Fail Anal 81:155–177. https://doi.org/10.1016/j.engfailanal.2017.08.003

Xu L (2014) Distribution and application of floor deviatoric stress tensor invariants under close-distance multiple pillars. China University of Mining and Technology, Beijing (**in Chinese**)

Xu L, Wei HX, Xiao Z, Li B (2015) Engineering cases and characteristics of deviatoric stress under coal pillar in regional floor. Rock Soil Mech. https://doi.org/10.16285/j.rsm.2015.02.036 (**in Chinese**)

Xu Y, Pan K, Zhang H (2019) Investigation of key techniques on floor roadway support under the impacts of superimposed mining: theoretical analysis and field study. Environ Earth Sci 78(15):436. https://doi.org/10.1007/s12665-019-8431-9

Yan H, Weng MY, Feng RM, Li WK (2015) Layout and support design of a coal roadway in ultra-close multiple-seams. J Cent South Univ 22(11):4385–4395. https://doi.org/10.1007/s11771-015-2987-7

Yang X, Wen G, Dai L, Sun H, Li X (2019) Ground subsidence and surface cracks evolution from shallow-buried close-distance multi-seam mining: a case study in Bulianta coal mine. Rock Mech Rock Eng 52(8):2835–2852. https://doi.org/10.1007/s00603-018-1726-4

Zhang M, Shimada H, Sasaoka T, Matsui K, Dou L (2014) Evolution and effect of the stress concentration and rock failure in the deep multi-seam coal mining. Environ Earth Sci 72(3):629–643. https://doi.org/10.1007/s12665-013-2985-8

Zhang W, Zhang D, Qi D, Hu W, He Z, Zhang W (2018) Floor failure depth of upper coal seam during close coal seams mining and its novel detection method. Energy Explor Exploit 36(5):1265–1278. https://doi.org/10.1177/0144598717747622

Zhou DQ, Jia Y, He SS, Han S (2016) Determination on reasonable position of roadway under boundary coal pillar in ultra contiguous seams. Coal Sci Technol S2:67–70 (**in Chinese**)

Zhu S, Lu L, Wu Y, Zhang T (2017a) Comprehensive study on the deformation and failure characteristics of a mining-impacted deep double-longwall working face floor. J Geophys Eng 14(3):641–653. https://doi.org/10.1088/1742-2140/aa64aa

Zhu GA, Dou LM, Wang CB, Li J, Cai W, Ding ZW (2017b) Numerical investigation of the evolution of overlying strata and distribution of static and dynamic loads in a deep island coal panel. Arab J Geosci. https://doi.org/10.1007/s12517-017-3300-x

**Publisher's Note** Springer Nature remains neutral with regard to jurisdictional claims in published maps and institutional affiliations.